Special Issue on Metamaterials EBG

Combinations of low/high permittivity and/or permeability substrates for highly directive planar metamaterial antennas

G. Lovat, P. Burghignoli, F. Capolino and D.R. Jackson

Abstract: An investigation of planar metamaterial antennas consisting of grounded metamaterial substrates with low and/or high values of the electric permittivity and/or the magnetic permeability excited by dipole sources is presented. Their performances are characterised in terms of their capability to radiate high levels of power density in the broadside direction and to produce narrow pencil beams pointing at broadside with high directivity. To achieve a high directivity, a pair of weakly attenuated cylindrical leaky waves is excited along the metamaterial substrate; sufficient conditions are established for the existence of such leaky waves in terms of the values of the substrate permittivity and permeability. Approximate closed-form expressions are derived for the phase and attenuation constants of the leaky waves. Numerical results are given in order to illustrate the radiative features of this class of antennas and to validate the theoretical analysis.

1 Introduction

Periodic structures made of metallic and/or dielectric inclusions in a uniform host medium may be represented, in suitable frequency ranges, as homogeneous artificial materials (metamaterials) that show novel and interesting electromagnetic features. One of these features is the creation of highly directive radiation beams from simple sources such as dipoles or slots placed inside such materials, as was obtained in the pioneering work of Gupta [1], Poilasne *et al.* [2] and Enoch *et al.* [3] For a detailed historical overview of such enhanced-directivity antennas, we address the reader to the Introduction of Lovat *et al.* [4]. The structures considered here consist of a grounded metamaterial layer that may have either high or low values of permittivity and/or permeability, excited by either an electric or a magnetic dipole source. Such structures are different from those where a cavity is created under a partially reflective surface that is formed by high-permittivity dielectrics [5–7], metallic FSS layers [8, 9] or other periodic dielectric structures [10, 11]. Although different in structure, the metamaterial antennas considered in this work are similar in terms of the mechanism of radiation: in fact, all the antennas in [1–11] radiate a narrow beam because the feed excites slowly attenuating leaky waves, as demonstrated in the work of Lovat *et al.* [4] and Jackson and Oliner [6].

The theory behind a grounded slab made of such metamaterials is revisited here, assuming a homogeneous isotropic medium with parameters μ_r, ε_r excited by a horizontal electric or magnetic dipole placed inside the slab or on the ground plane, respectively. The goal is to design planar antennas with a simple single-dipole feed featuring enhanced broadside radiation and/or very high directivity at broadside. Metamaterials are not usually isotropic when practically implemented, but the general properties discussed in this paper for the isotropic case, assumed for simplicity, have also been found assuming specific anisotropic models.

In this contribution, we focus on a comparison among antennas based on different realisations of substrates with high/low values of permittivity and/or permeability. The possibility of achieving high levels of radiated power density at broadside is ascertained, in connection with the values of the constitutive parameters of the substrate and of the electric or magnetic type of the source. Conditions for achieving the excitation of a pair of TE_z and TM_z leaky modes (where z is the direction orthogonal to the air–slab interface) with small and equal values of the phase and attenuation constants are then derived, which is a requirement for the radiation of a highly directive pencil beam pointing at broadside with a circular cross-section [12]. The conclusions given in this paper provide guidelines for a more comprehensive investigation assuming a more realistic homogeneous anisotropic model, or even the still further realistic case of a metamaterial made of actual periodic inclusions. Their importance rely also on the fact that no other studies have been carried out so far on this topic, and that the example seen in the literature represents just one of the possible choices (a low-permittivity metamaterial) that can be adopted in order to realise a planar radiator with enhanced directivity or broadside radiation.

For convenience of the reader, the terminology adopted throughout the paper for describing the various considered metamaterial media is reported here.

MNZ – mu near zero, that is, $|\mu_r| \ll 1$;
ENZ – epsilon near zero, that is, $|\varepsilon_r| \ll 1$;
MENZ – mu and epsilon near zero, that is, $|\mu_r| \ll 1$, and $|\varepsilon_r| \ll 1$;

doi:10.1049/iet-map:20050353

Paper first received 15th December 2005 and in revised form 20th July 2006

G. Lovat and P. Burghignoli are with the Electronic Engineering Department, 'La Sapienza' University of Rome, Via Eudossiana 18, Roma 00184, Italy

F. Capolino is with the Information Engineering Department, University of Siena, Via Roma 56, Siena 53100, Italy

D.R. Jackson is with the Department of Electrical and Computer Engineering, University of Houston, Houston, TX 77204-4005, USA

E-mail: capolino@ing.unisi.it

MVL – mu very large, that is, $|\mu_r| \gg 1$;
EVL – epsilon very large, that is, $|\varepsilon_r| \gg 1$;
Low-impedance material – $\eta_r = \sqrt{(\mu_r/\varepsilon_r)} \ll 1$;
High-impedance material – $\eta_r = \sqrt{(\mu_r/\varepsilon_r)} \gg 1$;
Low-index material – $n_r = \sqrt{(\mu_r\varepsilon_r)} \ll 1$;
High-index material – $n_r = \sqrt{(\mu_r\varepsilon_r)} \gg 1$.

2 Maximisation of broadside radiation

Let us consider a grounded slab as in Fig. 1, with constitutive parameters μ_r, ε_r, and thickness h, excited by a y-directed horizontal electric or magnetic dipole source placed at $z = h_s$ or on the ground plane, respectively. The electric far field radiated by the electric dipole source at broadside can be found by means of a simple application of the reciprocity theorem [5]. This is done by letting a y-polarised incident plane wave, having an amplitude of the electric field equal to $-jk_0\eta_0 \exp(-jk_0r)/(4\pi r)$ at the origin, impinge on the structure from broadside, and then calculating the reaction between the dipole source and the electric field inside the structure due to the incident plane wave. A similar analysis holds for the magnetic dipole source, using an x-polarised incident plane wave and taking the reaction between the dipole source and the resulting magnetic field inside the structure. The resulting broadside angular power density (W/steradian) at broadside ($\theta = 0$) is found to be

$$P_J(0) = \frac{k_0^2\eta_0}{8\pi^2} \frac{\eta_r^2 \sin^2(k_1h_s)}{\cos^2(k_1h) + \eta_r^2 \sin^2(k_1h)} \quad (1a)$$

$$P_M(0) = \frac{k_0^2}{8\pi^2\eta_0} \frac{1}{\cos^2(k_1h) + \eta_r^2 \sin^2(k_1h)} \quad (1b)$$

for a unit-amplitude electric dipole moment and for a unit-amplitude magnetic dipole moment, respectively, where $k_0 = \omega\sqrt{(\mu_0\varepsilon_0)}$, $\eta_0 = \sqrt{(\mu_0/\varepsilon_0)}$, $k_1 = k_0\sqrt{(\mu_r\varepsilon_r)}$ and $\eta_r = \sqrt{(\mu_r/\varepsilon_r)}$. The power density at broadside is investigated below assuming two cases: high- and low-impedance materials, since a large broadside power density requires one of these two cases.

Case 1: Materials with high intrinsic impedance. Considering metamaterial slabs with very high values of normalised intrinsic impedance, that is, with $\eta_r \gg 1$, it can easily be seen from (1) that, for both electric and magnetic sources, the broadside power density is maximised when $h = n\lambda_1/2$ (where $\lambda_1 = \lambda_0\sqrt{(\mu_r\varepsilon_r)}$ and $n = 1, 2, \ldots$). For an electric dipole, by letting $n = 1$ (which corresponds to the choice of the thinnest slab), the optimum source location is $h_s = h/2$, for which (1a) gives

$$P_J(0) = \frac{k_0^2\eta_0}{8\pi^2}\eta_r^2 \quad (2)$$

which can be made very large by increasing the normalised slab impedance η_r either by using an ENZ and/or a MVL material. A power enhancement factor E_P can be introduced as the ratio $E_{P,J} = P_J(0)/P_{J,0}(0)$ between the broadside power density radiated in the presence of the grounded slab $P_J(0)$ and that radiated in free space $P_{J,0}(0)$: the latter is equal to $P_{J,0}(0) = k_0^2\eta_0/(32\pi^2)$ W/steradian [13], so that in this case

$$E_{P,J} = 4\eta_r^2 \quad (3)$$

In contrast, for a magnetic dipole (whose broadside power density radiated in free space is equal to $P_{M,0}(0) = k_0^2/(32\pi^2\eta_0)$ W/steradian), (1b) yields

$$P_M(0) = \frac{k_0^2}{8\pi^2\eta_0} \quad (4)$$

that is independent of η_r. Hence a fixed enhancement factor $E_{P,M} = P_M(0)/P_{M,0}(0) = 4$ is obtained, which is the same as that due to the ground plane alone, and therefore no power enhancement at broadside is obtained from the metamaterial. It can be concluded that, for high-impedance slabs, electric sources must be employed in order to enhance broadside radiation.

Case 2: Materials with low intrinsic impedance. Conversely, considering metamaterial slabs with very low values of intrinsic impedance, that is, with $\eta_r \ll 1$, it can easily be seen from (1) that, for both electric and magnetic sources, the broadside power density is maximised when $h = (2n - 1)\lambda_1/4$ ($n = 1, 2, \ldots$). For an electric source, by letting $n = 1$, the optimum source location is $h_s = h$, for which (1a) gives the broadside power density as

$$P_J(0) = \frac{k_0^2\eta_0}{8\pi^2} \quad (5)$$

which is independent of η_r. In contrast, for a magnetic source, (1b) gives the broadside power density as

$$P_M(0) = \frac{k_0^2}{8\pi^2\eta_0\eta_r^2} \quad (6)$$

which can be made very large by decreasing the normalised slab impedance η_r either by using a MNZ and/or a EVL material. The relevant power enhancement factor is

$$E_{P,M} = \frac{4}{\eta_r^2} \quad (7)$$

It can be concluded that, for low-impedance slabs, magnetic sources must be employed in order to enhance broadside radiation.

3 Leaky waves and enhanced broadside directivity

As shown in the work of Ip and Jackson [12], the excitation on a planar structure of a pair of TE_z and TM_z cylindrical leaky waves that dominate the aperture field may produce a directive pencil-beam broadside radiation, that is, a beam pointing at broadside with equal beamwidths in the E and H planes. This will occur when each leaky wave has small and nearly equal values of the phase and attenuation constants (a requirement for a narrow pencil beam at broadside), and the wavenumbers and amplitudes of the two leaky waves are equal (this guarantees equal beamwidths in the principal planes). When the planar structure is excited by an actual source, the aperture field around the source is represented as the sum of surface waves and leaky waves (if any) and a term called the space wave, arising from the steepest-descent integration in the

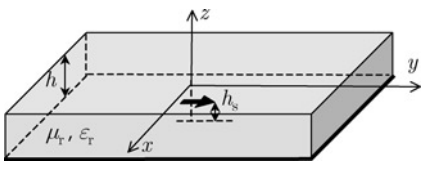

Fig. 1 *Grounded slab made of a homogeneous isotropic metamaterial, excited by a dipole source*

wavenumber plane [13, Ch. 5]. In most of the cases that correspond to a narrow-beam pattern, the aperture field is dominated by the leaky-wave contribution [4].

In what follows, sufficient conditions are derived for a grounded metamaterial slab to support such a pair of leaky waves, in terms of the physical parameters of the slab and the operating frequency.

3.1 Determination of the directive broadside radiation region in the μ_r–ε_r plane

The aim is to determine a region of the μ_r–ε_r plane in which a pair of TE$_z$ and TM$_z$ leaky modes with equal and small values of the phase and attenuation constants may propagate at the same frequency on a grounded metamaterial slab of thickness h and constitutive parameters μ_r, ε_r, so that approximately $\beta^{TE} = \alpha^{TE}$ and $\beta^{TM} = \alpha^{TM}$. As will be shown, the substrate parameters that give equality in the TE$_z$ case also give equality in the TM$_z$ case, so that the beam at broadside has equal E- and H-plane beamwidths. The dispersion equations to be studied are [14, Sec. 11.5]

$$\hat{k}_{z1}\cos(k_0 h\hat{k}_{z1}) + j\mu_r\hat{k}_{z0}\sin(k_0 h\hat{k}_{z1}) = 0 \quad (TE_z) \tag{8a}$$

$$\varepsilon_r\hat{k}_{z0}\cos(k_0 h\hat{k}_{z1}) + j\hat{k}_{z1}\sin(k_0 h\hat{k}_{z1}) = 0 \quad (TM_z) \tag{8b}$$

where $\hat{k}_{z0}$ and $\hat{k}_{z1}$ are the vertical wavenumbers in air and inside the slab, respectively, normalised with respect to the free-space wavenumber k_0; these are related to the radial modal propagation wavenumber $k_\rho = \beta - j\alpha = k_0\hat{k}_\rho$ through the relations $\hat{k}_{z0} = \sqrt{(1 - \hat{k}_\rho^2)}$ and $\hat{k}_{z1} = \sqrt{(n_r^2 - \hat{k}_\rho^2)}$.

Starting with the TE$_z$ case, it is assumed that at a certain frequency a TE$_z$ leaky mode exists with $\hat{k}_\rho^{TE} = (1 - j)\delta$, where δ is a complex parameter with a 'small' amplitude, that is, $|\delta^2| \ll 1$. Imposing also the restriction that $|\delta^2/n_r^2| \ll 1$ allows for the approximations $\hat{k}_{z0} \simeq 1 + j\delta^2$ and $\hat{k}_{z1} \simeq n_r + j\delta^2/n_r$, which come from the Taylor expansions for the vertical wavenumbers, for small δ and δ/n_r. As shown below, the assumptions that $|\delta^2| \ll 1$ and $|\delta^2/n_r^2| \ll 1$ lead to a self-consistent solution of the transcendental equation in (8a) for the wavenumber $\hat{k}_\rho$ for which δ is approximately real and small, and hence $\hat{\beta}^{TE} = \hat{\alpha}^{TE}$. The same procedure for the TM$_z$ leaky mode then reveals that $\hat{\beta}^{TM} = \hat{\alpha}^{TM}$ for precisely the same assumptions, and furthermore that $\hat{\beta}^{TE} = \hat{\alpha}^{TE} = \hat{\beta}^{TM} = \hat{\alpha}^{TM} = \hat{\alpha}$. This leads to the conclusion that a suitable range of permittivity and permeability values will result in a directive beam at broadside that has nearly equal beamwidths in the E and H planes. The allowed range of permittivity and permeability values define what is called the directive (pencil-beam) broadside radiation region (DBRR). This allowed range is derived below.

The beamwidths $\Delta\theta_{3dB}$ in the principal E and H planes can be expressed in terms of the attenuation constant as [12] $\Delta\theta_{3dB}|_E \simeq \Delta\theta_{3dB}|_H \simeq 2\sqrt{(2)}\hat{\alpha}$. The peak directivity at broadside is inversely proportional to the product of the beamwidths $\Delta\theta_{3dB}$ in the principal E and H planes, according to the approximate formula in [15, Eq. 2.27a], and thus we obtain

$$D_{max} \simeq \frac{9.87}{\Delta\theta_{3dB}|_E\Delta\theta_{3dB}|_H} \simeq \frac{1.23}{\hat{\alpha}^2} \tag{9}$$

where the normalised attenuation constant $\hat{\alpha}$ is found by solving (8).

Focusing on the TE$_z$ dispersion equation (8a), by using $\hat{k}_\rho^{TE} = (1 - j)\delta$ and approximating $\hat{k}_{z0}$ and $\hat{k}_{z1}$ in (8a) to first order in δ^2, it follows from (8a) that

$$\left(n_r + j\frac{\delta^2}{n_r}\right)\cos\left[k_0 h n_r\left(1 + j\frac{\delta^2}{n_r^2}\right)\right] + j\mu_r(1 + j\delta^2)\sin\left[k_0 h n_r\left(1 + j\frac{\delta^2}{n_r^2}\right)\right] = 0 \tag{10}$$

Consider now the particular cases illustrated in Section 2 for which a broadside power enhancement can be obtained. (It is not always necessary to have a high or low value of slab impedance in order to realise a directive beam, but the discussion here will be limited to these two important cases.) In Case 1 (high-impedance material), the operating frequency f_H is chosen so that $k_0 h n_r = \pi$ or equivalently $h = \lambda_0/(2n_r)$. Using this and keeping terms to order δ^2, the TE$_z$ dispersion relation (10) reduces to

$$\left(n_r + j\frac{\delta^2}{n_r}\right) - \pi\mu_r\left(\frac{\delta^2}{n_r^2}\right) = 0 \tag{11}$$

The solution of (11) is

$$\delta^2 = \frac{(\varepsilon_r^{3/2}\mu_r^{1/2}/\pi)}{1 - j\varepsilon_r/(\pi n_r)} \simeq \frac{\varepsilon_r^{3/2}\mu_r^{1/2}}{\pi} \tag{12}$$

where the last approximation is accurate provided that $\varepsilon_r/(\pi n_r) \ll 1$, or equivalently, $\pi\eta_r \gg 1$.

To be consistent with the initial hypothesis on δ^2, it is required that

$$|\delta^2| \ll 1 \Leftrightarrow \pi\sqrt{\frac{\mu_r}{\varepsilon_r}}\left(\frac{\varepsilon_r}{\pi}\right)^2 \ll 1 \tag{13a}$$

$$\left|\frac{\delta^2}{n_r^2}\right| \ll 1 \Leftrightarrow \pi\sqrt{\frac{\mu_r}{\varepsilon_r}} \gg 1 \tag{13b}$$

Note that the approximation made in (12) is accurate since we are assuming that (13b) is satisfied. Equations (13) thus represent a sufficient condition to have δ be approximately real and very small, and hence $\hat{\beta}^{TE} = \hat{\alpha}^{TE} = \delta$, which implies having a narrow beam in the H plane. It is clear that (13b) is automatically satisfied under the assumption of a high-impedance material, which requires the use of either an ENZ or a MVL slab. Equation (13a) then implies that a high directivity is only possible for an ENZ slab. When (13) hold, they yield the result

$$\hat{\beta}^{TE}\Big|_{f=f_H} = \hat{\alpha}^{TE}\Big|_{f=f_H} \simeq \sqrt{\pi\sqrt{\frac{\mu_r}{\varepsilon_r}}\left(\frac{\varepsilon_r}{\pi}\right)^2} = \frac{1}{\sqrt{\pi}}\frac{n_r}{\sqrt{\eta_r}} \tag{14}$$

By means of the same analysis carried out for the TE$_z$ case, results may also be obtained for the TM$_z$ case, starting from (8b) (the details are omitted for brevity). In particular, the same result expressed by (14) is also found for the TM$_z$ case, along with the same restrictions on the substrate parameters that were found for the TE$_z$ case (see (13)). This implies that when the inequalities in (13) are satisfied an equally narrow beamwidth is obtained in the E and H planes, with a peak directivity (at broadside) that is $D_{max} \simeq 3.88\eta_r/n_r^2 = 3.88/(\mu_r\varepsilon_r^3)^{1/2}$.

In Case 2 (low-impedance material), the operating frequency f_L is chosen so that $k_0 h n_r = \pi/2$, or equivalently $h = \lambda_0/(4n_r)$. Starting again from (10) for the TE$_z$ case and reasoning as for the high-impedance case, the result is

$$\delta^2 = \frac{(2/\pi)\mu_r^{3/2}\varepsilon_r^{1/2}}{1 - j((2/\pi)\mu_r^{3/2}\varepsilon_r^{1/2})} \simeq \frac{2}{\pi}\mu_r^{3/2}\varepsilon_r^{1/2} \tag{15}$$

where the last approximation is accurate provided that $(2/\pi)\mu_r^{3/2}\varepsilon_r^{1/2} \ll 1$. Again, to be consistent with the initial hypotheses on $|\delta^2|$, it is required that

$$|\delta^2| \ll 1 \Leftrightarrow \frac{2}{\pi}\mu_r^{3/2}\varepsilon_r^{1/2} = \left(\frac{2}{\pi}\sqrt{\frac{\mu_r}{\varepsilon_r}}\right)^{-1}\left(\frac{2}{\pi}\mu_r\right)^2 \ll 1 \quad (16a)$$

$$\left|\frac{\delta^2}{n_r^2}\right| \ll 1 \Leftrightarrow \frac{2}{\pi}\sqrt{\frac{\mu_r}{\varepsilon_r}} \ll 1 \quad (16b)$$

Note that the approximation made in (15) is accurate since we are assuming that (16a) is satisfied. Equation (16b) is automatically satisfied under the assumption of a low-impedance material, which requires the use of either an MNZ or an EVL slab. Equation (16a) implies that a high directivity can only be achieved by using an MNZ slab. When (16) hold, they yield

$$\hat{\beta}^{TE}\Big|_{f=f_L} = \hat{\alpha}^{TE}\Big|_{f=f_L} \simeq \sqrt{\left(\frac{2}{\pi}\sqrt{\frac{\mu_r}{\varepsilon_r}}\right)^{-1}\left(\frac{2}{\pi}\mu_r\right)^2} = \sqrt{\frac{2}{\pi}}n_r\sqrt{\eta_r} \quad (17)$$

Omitting the details once again, the same results and restrictions as shown in (16) and (17) are obtained for the TM_z case. This implies a symmetric pencil beam at broadside, as for Case 1, with a directivity $D_{max} \simeq 1.94/(n_r^2\eta_r) = 1.94/(\mu_r^3\varepsilon_r)^{1/2}$. It should be noted that, for dual values of μ_r and ε_r, employing MNZ media allows to use thinner slabs with respect to ENZ media, although, by comparing (14) and (17), in the former case the attenuation constant is larger (hence the beam is less directive) by a factor $\sqrt{2}$. It is also worth noting that the possible use of high-index (EVL or MVL) media reduces considerably the normalised thickness of the slab h/λ_0.

The results of the previous analysis are reported in Table 1. By somewhat arbitrarily assuming the values 0.1 and 10 as upper and lower limits for values much smaller or much higher than 1, respectively, conditions (13) and (16) for having very small $\hat{\beta}^{TE} = \hat{\alpha}^{TE} = \hat{\beta}^{TM} = \hat{\alpha}^{TM}$ can be written as

$$\begin{cases} \mu_r \le \dfrac{\pi^2}{100\varepsilon_r^3} \\ \mu_r \ge \dfrac{100\varepsilon_r}{\pi^2} \end{cases} (f = f_H) \qquad \begin{cases} \mu_r \le \sqrt[3]{\dfrac{\pi^2}{400\varepsilon_r}} \\ \mu_r \le \dfrac{\pi^2}{400}\varepsilon_r \end{cases} (f = f_L) \quad (18)$$

Taken together, these set of inequalities determine the region of the μ_r–ε_r plane that is the DBRR. A sketch of such a region is reported in Fig. 2 (the shaded region) on a bi-logarithmic scale together with the high- and low-index regions, and the high- and low-impedance regions (defined in the figure somewhat arbitrarily as $n_r \ge 10$ and $n_r \le 0.1$, and $\eta_r \ge 10$ and $\eta_r \le 0.1$, respectively). Note that the boundaries of the DBRR are, however, only approximate because of the somewhat arbitrary limits adopted in connection with (18). Furthermore, because of the definitions adopted for high/low impedance in Fig. 2, the DBRR region in Fig. 2 extends beyond the defined limits of the high-impedance region (due to the factor of π in (13b) and $2/\pi$ in (16b)). The DBRR region gives the region of high directivity at broadside. If a particular slab material lies within the DBBR, then a directive beam may be obtained. It is observed that neither the value of the normalised impedance η_r nor the value of the normalised index n_r alone determine whether the slab material lies inside the DBRR, but both of them. The power density radiated at broadside can be maximised by using either a horizontal electric dipole or a horizontal magnetic dipole, depending on whether the point lies above or below the central band of the DBRR region.

Table 1: Sufficient conditions for directive broadside radiation, relevant expressions for the leaky-wave phase and attenuation constants, and broadside power enhancement factors

$h = \lambda_1/2$ ($f = f_H$)	$h = \lambda_1/4$ ($f = f_L$)
$\pi\eta_r \gg 1$ and $\pi\eta_r(\varepsilon_r/\pi)^2 \ll 1$ high impedance material, ENZ	$(2/\pi)\eta_r \ll 1$ and $((2/\pi)\eta_r)^{-1}((2/\pi)\mu_r)^2 \ll 1$ low impedance material, MNZ
$\hat{\beta} = \hat{\alpha} \simeq \sqrt{(\pi\eta_r(\varepsilon_r/\pi)^2)} = (1/\sqrt{(\pi)})n_r/\sqrt{(\eta_r)}$	$\hat{\beta} = \hat{\alpha} \simeq \sqrt{(((2/\pi)\eta_r)^{-1}((2/\pi)\mu_r)^2)} = \sqrt{(2/\pi)}n_r\sqrt{(\eta_r)}$
$E_{P,J} = 4\eta_r^2$ (electric dipole in the middle of the slab)	$E_{P,M} = 4/\eta_r^2$ (magnetic dipole on the ground plane)

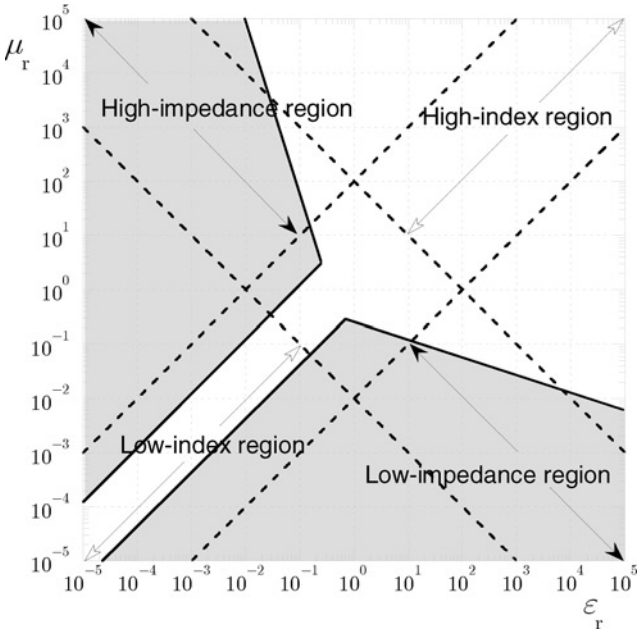

Fig. 2 DBRR *(dark shaded area) in the μ_r–ε_r plane for a grounded metamaterial slab excited by a horizontal dipole source*
The DBRR is the region of high broadside directivity, under the assumption that the impedance of the slab is either high or low

As already noted in Section 1, these results provide guidelines useful for investigating more complicated and realistic models that would take into account the anisotropy and possibly also the non-linearity or the spatial dispersion of the medium. Examples of such media presenting very high and/or very low values of the constitutive parameters are ferroelectric thin films (very large permittivities) [16], ferrimagnetic layers (very large or very low permeabilities, depending on the operating frequency) and plasma layers (very low positive or very large negative permittivities). Among the artificial materials, other examples are provided by wire media (very low positive or very large negative permittivities) [17], metaferrites (very low positive or very large permeabilities) [18] and other structures obtained by suitably combining the above-mentioned materials.

3.2 Numerical examples

To validate the above analysis, in this section we show dispersion and radiation features of grounded metamaterial

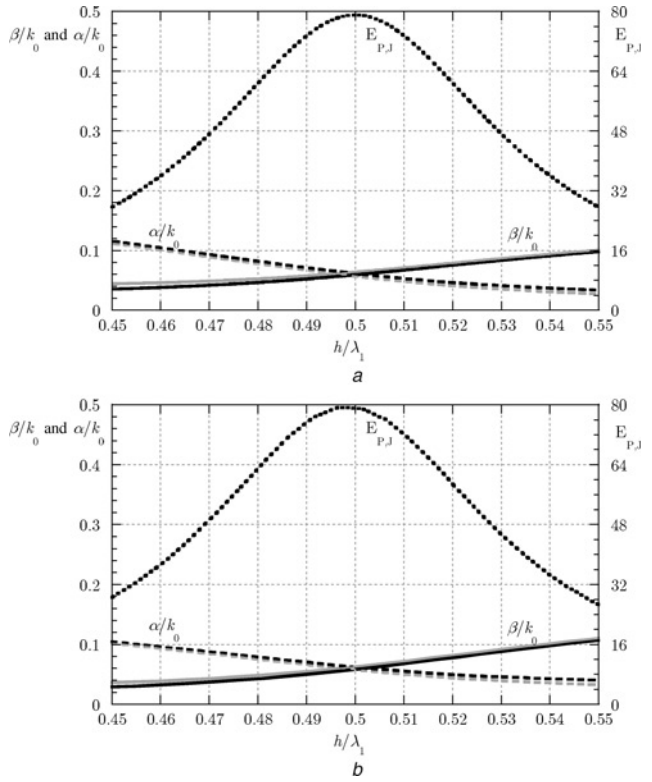

Fig. 3 *Normalised phase (solid lines) and attenuation (dashed lines) constants of the fundamental TM_z (black lines) and TE_z (gray lines) leaky modes, and broadside power enhancement factor $E_{P,J}$ (black dotted lines), for a grounded metamaterial slab as in Fig. 1 excited by an electric dipole source, as a function of the normalised slab thickness*

a Non-dispersive metamaterial with $\varepsilon_r = 0.05060$
b Plasma-like metamaterial with $h = 33.32$ mm and $f_p = 19.49$ GHz
Other parameters: $\mu_r = 1$, $h_s = h/2$

slabs with different geometrical and ideal physical parameters (permittivity and permeability) inside the DBRR.

In Fig. 3, the normalised phase and attenuation constants (β/k_0 and α/k_0) together with the broadside enhancement factor $E_{P,J}$ are reported as functions of the normalised slab thickness h/λ_1 for a grounded ENZ slab excited by an electric dipole placed in the middle of the slab. In Fig. 3*a*, the case of a non-dispersive metamaterial with $\mu_r = 1$ and $\varepsilon_r = 0.05060$ is considered: this corresponds to a nominally high impedance ($\eta_r = 4.45$) and nominally low permittivity point inside the DBRR. In Fig. 3*b*, a dispersive metamaterial is used with a plasma-like permittivity $\varepsilon_r(f) = 1 - f_p^2/f^2$ and plasma frequency $f_p = 19.49$ GHz. In Fig. 3*b*, a fixed slab thickness $h = 33.32$ mm has been used along with a variable frequency, so that h/λ_1 is a function of frequency. The value of the plasma frequency has been chosen in order to have the same relative permittivity ($\varepsilon_r = 0.05060$) as in the dispersionless case for the frequency (20 GHz) that corresponds to the optimum thickness $h/\lambda_1 = 0.5$. It can be observed that in both cases the TE_z and TM_z leaky waves have approximately the same value of the propagation wavenumber for $h/\lambda_1 = 0.5$ where the broadside enhancement factor $E_{P,J}$ has its maximum, as expected from the analysis in Section 2. Moreover, the approximate values for $\hat{\beta}$ and $\hat{\alpha}$ calculated through the expressions reported in Table 1 are $\hat{\beta} = \hat{\alpha} \simeq 0.0602$, in excellent agreement with the exact ones, $\hat{\beta}^{TM} = 0.0595$, $\hat{\alpha}^{TM} = 0.0616$, $\hat{\beta}^{TE} = 0.0637$ and $\hat{\alpha}^{TE} = 0.0572$. The exact value of the maximum $E_{P,J}$ in the dispersive case is 79.42 (which occurs exactly at $h/\lambda_1 = 0.4975$), whereas the value from

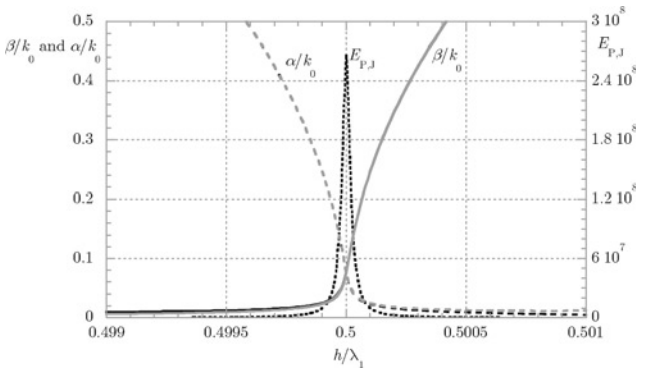

Fig. 4 *Same as in Fig. 3a for a grounded metamaterial slab with constitutive parameters $\varepsilon_r = 1.5 \times 10^{-3}$, $\mu_r = 1 \times 10^5$, which is excited by an electric dipole source placed at $h_s = h/2$*

Table 1 is $E_{P,J} = 79.05$ (which coincides exactly with the maximum value obtained in the non-dispersive case). It can also be observed that the leaky-wave propagation wavenumbers and the broadside enhancement factor $E_{P,J}$ are very similar in the non-dispersive and dispersive cases, since the value of the plasma frequency has been chosen in order to have the same relative permittivity at the optimum frequency for which $h/\lambda_1 = 0.5$. However, by varying the frequency (results omitted) it can be seen that the 3 dB frequency bandwidth for the broadside power density is very different, being equal to 14.7% in the non-dispersive case and 0.73% in the dispersive case. This aspect is discussed in more detail in the work of Lovat *et al.* [19].

In Fig. 4 a metamaterial that is both ENZ and MVL ($\varepsilon_r = 1.5 \times 10^{-3}$ and $\mu_r = 1 \times 10^5$) is considered, still excited by an electric dipole source placed in the middle of the slab. This corresponds to a very high-impedance ($\eta_r = 8165$) and very low-permittivity point inside the DBRR. Once again, it can be noted that for $h/\lambda_1 = 0.5$ the leaky-wave phase and attenuation constants are approximately equal and the $E_{P,J}$ factor has a maximum. As in the previous case, the approximate values of the leaky-wave propagation wavenumbers at the broadside-radiation point found from Table 1 ($\hat{\beta} = \hat{\alpha} \simeq 0.076$) are in excellent agreement with the ones calculated numerically, and the maximum $E_{P,J}$ factor is very large, being $E_{P,J} \simeq 2.67 \times 10^8$.

In Fig. 5 a grounded MNZ ($\varepsilon_r = 1.2$ and $\mu_r = 0.01$) slab is considered. This case corresponds to a moderately low-impedance ($\eta_r = 0.091$) and moderately low-permeability point inside the DBRR. In this case, for $h/\lambda_1 = 0.25$ the leaky-wave phase and attenuation constants are

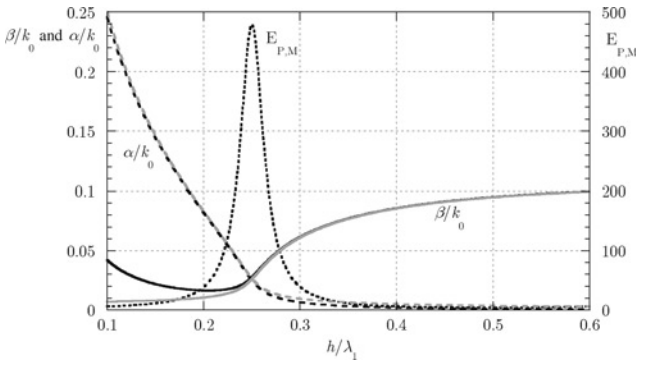

Fig. 5 *Normalised phase (solid lines) and attenuation (dashed lines) constants of the fundamental TM_z (black lines) and TE_z (gray lines) leaky modes for a grounded metamaterial slab with constitutive parameters $\mu_r = 0.01$ and $\varepsilon_r = 1.2$ as a function of the normalised slab thickness*

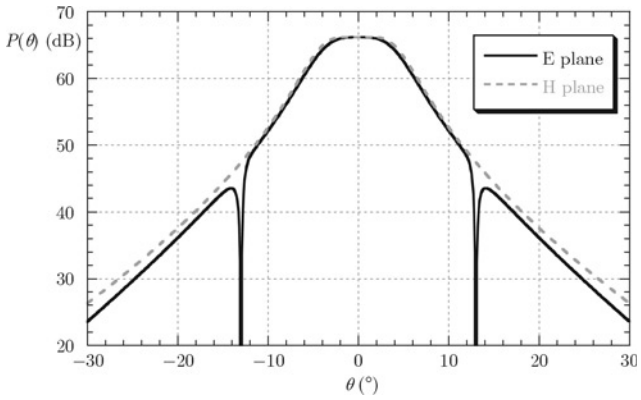

Fig. 6 *E-plane (solid black line) and H-plane (dashed gray line) radiation patterns for a structure as in Fig. 3b with h = 33.32 mm at f = f_H ≡ 20 GHz*

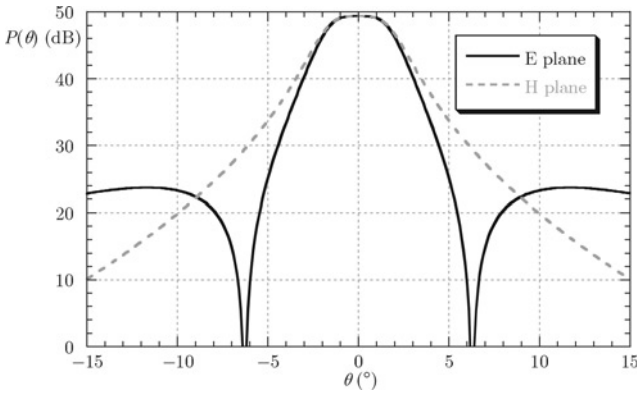

Fig. 8 *E-plane (solid black line) and H-plane (dashed gray line) radiation patterns for a structure as in Fig. 5 with h = 75 mm excited by an electric dipole source placed in the middle of the slab at f = f_L ≡ 9.122 GHz*

approximately equal, and exciting the slab with a magnetic dipole on the ground plane the $E_{P,M}$ factor has a maximum, as expected; the relevant approximate values of the leaky-wave propagation wavenumbers found from Table 1 are $\hat{\beta} = \hat{\alpha} \simeq 0.026$, whereas the maximum $E_{P,M}$ factor is $E_{P,M} \simeq 480$.

In Figs. 6, 7, and 8, radiation patterns in the principal planes are shown for the same structures of Figs. 3*b*, 4 and 5, respectively, in order to show the occurrence of directive broadside radiation. In all cases the excitation is an electric dipole placed in the middle of the slab. As noted in Table 1, the operating frequencies are f_H for Figs. 6 and 7, and f_L for Fig. 8 (the latter being an MNZ structure).

In Fig. 6, the slab thickness is fixed at $h = 33.32$ mm and the operating frequency is $f_H = 20$ GHz. As expected, a highly directive pencil beam is radiated; in particular, the H- and E-plane radiation patterns are almost superimposed in the shown angular range, except for a narrow dip occurring in the E-plane pattern due to a destructive interference with radiation from an additional subdominant TM_z leaky mode.

In Fig. 7, the slab thickness is fixed at $h = 1$ mm and the operating frequency is $f = f_H \equiv 12.24$ GHz $(h/\lambda_1 = 0.5)$. Again, a highly directive pencil beam with equal beamwidths in the principal planes can be observed. In this case no dip is present in the E plane since, for the choice of the slab parameters, the contribution of the additional TM_z leaky mode is completely negligible.

In Fig. 8, the slab thickness is fixed at $h = 75$ mm and the operating frequency is $f = f_L \equiv 9.122$ GHz $(h/\lambda_1 = 0.25)$. The disagreement between the E- and H-plane patterns outside of the peak region is larger in this case. However, this can be explained by keeping in mind that the structure is excited at the frequency f_L by an electric dipole, so that no power enhancement is produced, according to the explanation in Section 2. Although weakly attenuated leaky waves are still excited by the source along the surface of the substrate, the direct non-modal radiation from the source (i.e. the space wave [13, Ch. 5]) in the E plane is not negligible, and it radiates an appreciable broad beam. Near broadside the patterns are still dominated by the large equivalent-aperture field distribution due to the leaky waves (TE_z and TM_z). Away from broadside, a dip in the E-plane pattern is also present due to the destructive interference between the space-wave and the leaky-wave contributions to the far field. To recover the same situation of Fig. 7 (where the total field is very much dominated by the leaky-wave field alone), a magnetic dipole on the ground plane is used to excite the antenna and the corresponding radiation pattern is reported in Fig. 9, where the patterns in the principal planes are superimposed and the level of the radiated power density is greatly enhanced, as expected. The directivity of the cases in Figs. 8 and 9 is comparable, but the power density at broadside in Fig. 9 is much higher than that in Fig. 8.

Finally, in Fig. 10 we consider the case of a structure designed to have a broadside power enhancement (according to (2)) whose constitutive parameters lie outside the DBRR of Fig. 2. As an example, the parameters are $\varepsilon_r = 2$, $\mu_r = 200$ and $h = 0.3750$ mm, and the excitation

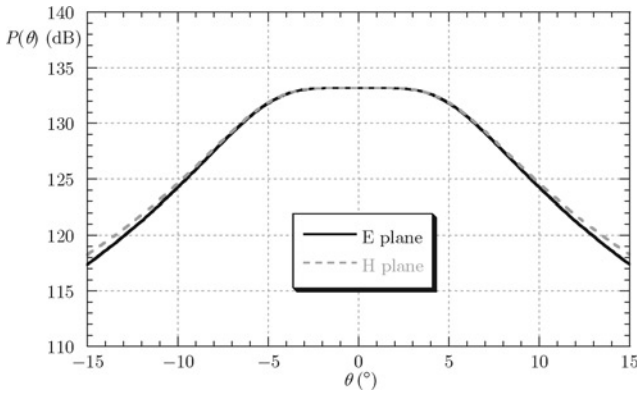

Fig. 7 *E-plane (solid black line) and H-plane (dashed gray line) radiation patterns for a structure as in Fig. 4 with h = 1 mm at f = f_H ≡ 12.24 GHz*

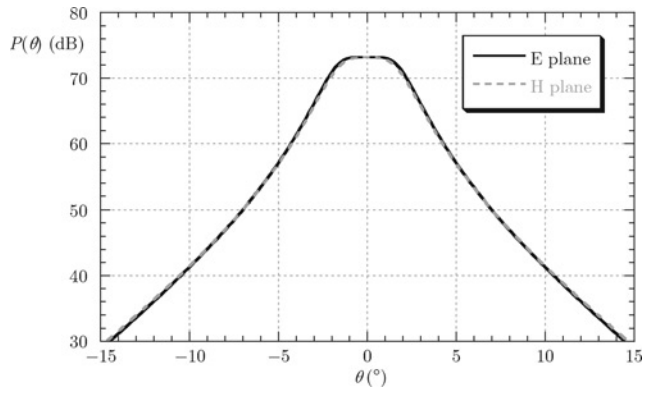

Fig. 9 *Same as in Fig. 8, but with a magnetic dipole source on the ground plane*

Directivity is comparable with that of Fig. 8, but the power at broadside is much higher

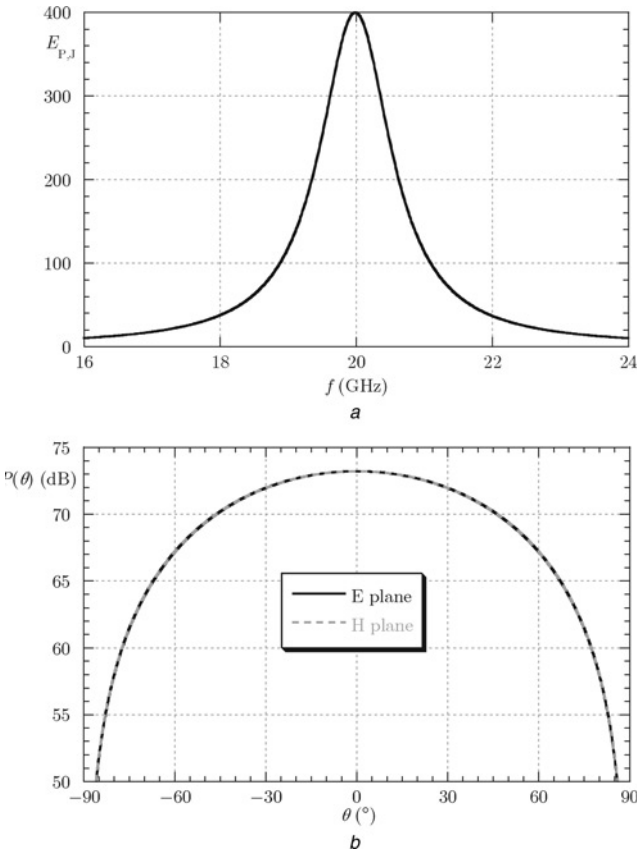

Fig. 10 *Grounded metamaterial slab with parameters $\varepsilon_r = 2$, $\mu_r = 200$ (lying outside the DBRR of Fig. 2) and $h = 0.3750$ mm, excited by an electric dipole source placed in the middle of the slab*

a Broadside enhancement factor $E_{P,J}$ as a function of frequency with maximum at $f = f_H \equiv 20$ GHz
b Non-directive E-plane (solid black line) and H-plane (dashed gray line) radiation patterns at $f = f_H \equiv 20$ GHz

is an electric dipole. In Fig. 10*a*, the $E_{P,J}$ factor as a function of frequency is shown and it has a maximum equal to 400 at the frequency $f = f_H \equiv 20$ GHz; however, in this case no physical leaky mode exists, and thus no directive radiation is to be expected. This is verified in Fig. 10*b*, where both the E- and H-plane patterns are seen to be very broad.

5 Conclusion

Grounded metamaterial slabs have been studied with the aim of designing planar antennas with enhanced broadside radiation and/or high broadside directivity. Ideal isotropic and homogeneous media have been assumed, examining various combinations of high/low permittivity and permeability. Conditions were derived for maximising the power density radiated at broadside by simple electric or magnetic dipole sources. This requires that the intrinsic impedance of the metamaterial be either high (for an electric dipole source) or low (for a magnetic dipole source). The optimum slab thickness is then a half wavelength or a quarter wavelength, respectively. A class of configurations capable of producing narrow omnidirectional beams pointing at broadside was then identified by requiring the presence of a pair of TE_z and TM_z weakly attenuated leaky waves with the same values of the phase and attenuation constants. This allows for a range for the substrate constitutive parameters to be defined that gives rise to directive broadside radiation. The main results from this analysis are summarised in Fig. 2 and Table 1, which show the ranges of relative permittivity and permeability necessary to give a highly directive pattern when using a planar metamaterial substrate, under the assumption that the slab intrinsic impedance is either high or low. (It may be possible to obtain high directivity using impedances that are neither high nor low, but this was not explored here.) Interestingly, high directivity can be obtained using a slab material that has a low, moderate or high value of refractive index, if the combination of permittivity and permeability is chosen properly. Note that previous high-directivity metamaterial antennas used low-index metamaterials [1, 3, 4].

6 Acknowledgment

The support of the EU-funded project METAMORPHOSE (FP6/NMP3-CT-2004-500252) is gratefully acknowledged.

7 References

1 Gupta, K.C.: 'Narrow-beam antennas using an artificial dielectric medium with permittivity less than unity', *Electron. Lett.*, 1971, **7**, (1), pp. 16–18
2 Poilasne, G., Pouliguen, P., Lenormand, J., Mahdjoubi, K., Terret, C., and Gelin, P.: 'Theoretical study of interactions between antennas and metallic photonic bandgap materials', *Microw. Opt. Technol. Lett.*, 1997, **15**, (6), pp. 384–389
3 Enoch, S., Tayeb, G., Sabouroux, P., Guérin, N., and Vincent, P.: 'A metamaterial for directive emission', *Phys. Rev. Lett.*, 2002, **89**, (21), p. 213902-1–213902-4
4 Lovat, G., Burghignoli, P., Capolino, F., Jackson, D.R., and Wilton, D.R.: 'Analysis of directive radiation from a line source in a metamaterial slab with low permittivity', *IEEE Trans. Antennas Propag.*, 2006, **54**, (3), pp. 1017–1030
5 Jackson, D.R., and Alexópoulos, N.G.: 'Gain enhancement methods for printed circuit antennas', *IEEE Trans. Antennas Propag.*, 1985, **33**, (9), pp. 976–987
6 Jackson, D.R., and Oliner, A.A.: 'A leaky-wave analysis of the high-gain printed antenna configuration', *IEEE Trans. Antennas Propag.*, 1988, **36**, (7), pp. 905–910
7 Jackson, D.R., Oliner, A.A., and Ip, A.: 'Leaky-wave propagation and radiation for a narrow-beam multiple-layer dielectric structure', *IEEE Trans. Antennas Propag.*, 1993, **41**, (3), pp. 344–348
8 Von Trentini, G.: 'Partially reflecting sheet arrays', *IEEE Trans. Antennas Propag.*, 1956, **4**, (10), pp. 666–671
9 Feresidis, A.P., and Vardaxoglou, J.C.: 'High gain planar antenna using optimised partially reflective surfaces', *IEE Proc., Microw. Antennas Propag.*, 2001, **148**, (6), pp. 345–350
10 Temelkuran, B., Bayindir, M., Ozbay, E., Biswas, R., Sigalas, M.M., Tuttle, G., and Ho, K.M.: 'Photonic crystal-based resonant antenna with a very high directivity', *J. Appl. Phys.*, 2000, **87**, (1), pp. 603–605
11 Fehrembach, A., Enoch, S., and Sentenac, A.: 'Highly directive light sources using two-dimensional photonic crystal slabs', *Appl. Phys. Lett.*, 2001, **79**, (26), pp. 4280–4282
12 Ip, A., and Jackson, D.R.: 'Radiation form cylindrical leaky waves', *IEEE Trans. Antennas Propag.*, 1990, **38**, (4), pp. 482–488
13 Felsen, L.B., and Marcuvitz, N.: 'Radiation and scattering of waves' (IEEE Press, Piscataway, NJ, 2003)
14 Collin, R.E.: 'Field theory of guided waves' (IEEE Press, Piscataway, NJ, 1991, 2nd edn.)
15 Balanis, C.A.: 'Antenna theory' (Wiley, New York, NY, 1997)
16 Liu, S.W., Lin, Y., Weaver, J., Donner, W., Chen, X., Chen, C.L., Jiang, J.C., Meletis, E.I., and Bhalla, A.: 'High-dielectric tunability of ferroelectric (Pb,Sr)TiO_3 thin films on (0 0 1) $LaAlO_3$', *Appl. Phys. Lett.*, 2004, **85**, (15), pp. 3202–3204
17 Silveirinha, M.G., and Fernandes, C.A.: 'Homogenization of 3-D-connected and nonconnected wire metamaterials', *IEEE Trans. Microw. Theory Tech.*, 2005, **53**, (4), pp. 1418–1430
18 Kern, D.J., and Werner, D.H.: 'Metaferrites: using electromagnetic bandgap to synthesize metamaterial ferrites', *IEEE Trans. Antennas Propag.*, 2005, **53**, (4), pp. 1382–1389
19 Lovat, G., Burghignoli, P., Capolino, F., and Jackson, D.R.: 'Highly directive planar leaky-wave antennas: a comparison between metamaterial-based and conventional designs', *Proc. European Microwave Association* 2006, **2**, (2), pp. 12–21 (Special issue on microwave metamaterials: theory, fabrication and applications)